10   Phase transitions, thermal transport and new materials

R. Dell'Amore, A. Engel (since August 2004), M. Reibelt, A. Schilling

in collaboration with:
Ch. Rüegg, Paul Scherrer Institute, K. Krämer, University of Bern, G. Ravikumar, Bhaba Atomic Research Center, Th. Wolf, Forschungszentrum Karlsruhe, K. Il'in, Universität Karlsruhe, P. Canfield, Iowa State University, J. Karpinksi, ETH Zürich, H.-W. Hübers, Deutsches Zentrum für Luft- und Raumfahrt, CSEM Neuenburg, FIRST Lab ETH Zürich.

Besides various activities to extend our experimental possibilities and to complete the equipment used by all the members of our group, we have started a new activity, the study of superconducting thin-film nanostructures. Nanostructuring of materials in general has become a more and more widely used technique to do state-of-the-art experiments. Some of our group members are trained at the FIRST Center for Micro- and Nanoscience at the ETH Zürich, which will enable us to act more flexibly if new developments in solid-state physics require the micro- or nanostructuring of samples or experiments.

10.1   Physics of superconducting thin-film nanostructures and possible applications as fast single-photon detectors

10.1.1   Motivation

Besides the obvious applications of superconducting materials in the field of loss-free current distribution and energy storage the unique properties of the superconducting state also open up a very wide field of electronic and detector applications. In this new project we aim at exploring the physics of narrow superconducting strips and their potential as single-photon detectors eventually covering a spectral range from infrared to high-energy x-ray photons.

Scientific progress always demands faster, more sensitive detectors with a higher energy resolution, ideally all combined within one device that is even scalable to a multi-pixel imaging camera. The recently proposed design of a superconducting single-photon detector (1) based on thin and narrow superconducting strips has promise of better performance with respect to various applications compared to existing technologies. Absorption of a photon in a superconductor leads to the breakage of a Cooper-pair. In general, the photon energy is orders of magnitude larger than the superconducting gap energy, thus creating a highly-excited, non-equilibrium electron. The cascade-like thermalization process results in a large number of quasiparticles within an extremely short timescale on the order of femtoseconds. The thus formed hot-spot has a size that is determined by the photon energy, quasi-particle multiplication efficiency, diffusion of quasi-particles, their decay via recombination and phonon escape into the substrate and the dimensions of the superconductor. Within the hot-spot superconductivity is weakened or even completely suppressed. In a bulk superconductor the hot-spot usually goes unnoticed except when the temperature is right at the superconducting transition and for relatively high photon flux.
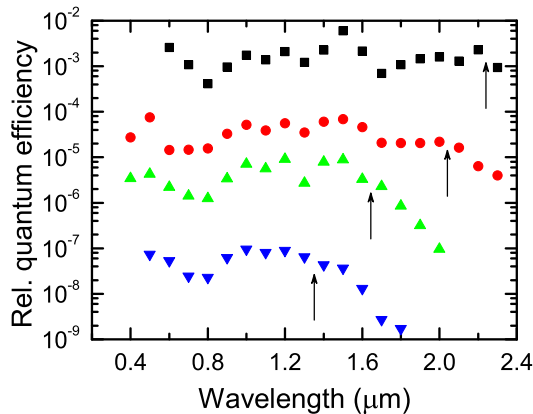
Figure 10.1:
Signal count rates for a photon detector made from a NbN thin film as a function of the wavelength of the incident light. Data were taken for different bias currents; from bottom to top they were set to 0.6, 0.77, 0.8 and 0.89 times the critical current at the operating temperature. For clarity, the data have been shifted along the vertical axis. The cut-off wavelengths are marked by arrows.

In two-dimensional NbN thin-films the hot spot reaches a radius of about 10 nm after absorption of an optical photon. Structures of such narrow dimensions are still out of reach of standard lithography. However, applying a bias current only slightly less than the critical current of the strip, optical and near-infrared photons can be readily detected in 100 nm wide strips, a size achievable using e-beam lithography. The effect of the hot-spot formation may be macroscopically described as a localized reduction of the effective critical current density. If it drops below the applied current density, a complete cross-section of the strip switches temporarily into the normal state and a voltage transient develops between the strip ends.

10.1.2 Photon detection and fluctuations

The original detection model is based on the formation of a normal conducting core within the hot-spot. If the size of this normal core is larger than the superconducting coherence length the applied bias current is redistributed which eventually leads to the formation of the voltage transient. Inherent to this model is a long wavelength cut-off; photons with $\lambda > \lambda_{\text{cut-off}}$ result in hot-spots with a normal core that is too small to trigger the signal. Multi-photon or fluctuation assisted processes may still result in a positive detection event, but with a substantially reduced probability. At higher photon energies, i.e. shorter wavelengths the detection probability should be relatively flat, resembling the absorption probability of these photons within the superconducting strip. The plateau in the detection efficiency at short wavelengths has been experimentally confirmed (see Fig. 10.1) and also the decrease beyond a bias current dependent cut-off wavelength (2). However, the cut-off is not sharp but rather rounded and continuous. Furthermore, knowledge of the dependence of the cut-off wavelength on bias current allows one to calculate the theoretical normal core size of the hot-spot as a function of the photon wavelength. It turns out that these core sizes are far too large in comparison to model estimates (3).

These apparent contradictions prompted us to advance the detection model (4). The key point in our refined detection model is that the formation of a normal core within the hot-spot is not even necessary to trigger a voltage pulse. Instead we considered the reduction of the Cooper-pair density within a cross-section of the superconducting strip that is centered around the point of photon absorption. We could show that a certain number of Cooper-pairs need to be broken for a positive detection event, which is equivalent to a local reduction of the critical current density below the applied current density. Model calculations have shown, that this happens well before the normal conducting core of the hot-spot has
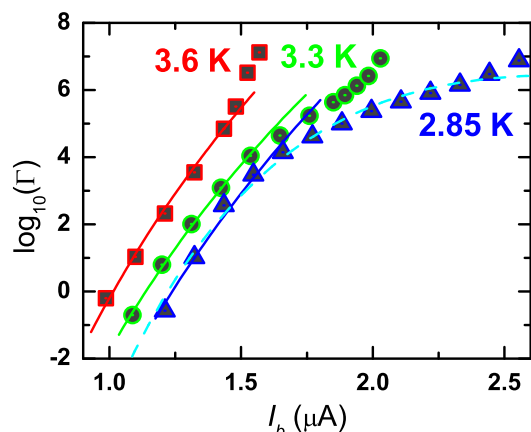
Figure 10.2:
Dark count rates as a function of bias current for different operating temperatures. The dark count rates exhibit a strong current and peculiar temperature dependence. The curves are calculated according to a model based on fluctuating vortex-antivortex pairs. Such a model seems to be promising to explain the observed behavior.

formed and gives a much more consistent description of the experimental data.

Another important issue we have recently addressed are fluctuations of the superconducting order parameter in these nanostructures that make up these photon detectors and which are a major source of dark count events. In Fig. 10.2 signal counts that were recorded with no incident light on the detectors are plotted versus the applied bias current for three different temperatures. There are a whole range of effects that might be responsible for fluctuations that could cause voltage pulses to develop even in the absence of photons. But a deeper analysis of the distinct temperature and current dependence leaves just a few effects as likely candidates able to describe the experimental data. We suggest fluctuating vortex-antivortex pairs as the main source of dark count events (5). In two-dimensional superconductors the occurrence of such vortex pairs is well established and due the Lorentz force caused by the applied current, these pairs may break and start to move towards opposite edges of the strip. This movement in turn will cause a voltage pulse quite similar to those caused by absorbed photons. At high temperatures this model fits the experimental data quite well already. Tweaking the model parameters a little bit, the fit at lower temperatures can improved substantially (dashed curve in Fig. 10.2), however, at the current state, this is purely phenomenological and not based on a sound theoretical model.

10.1.3   Outlook

Improving the detector performance in terms of detection efficiency and spectral range is necessary if such detectors should become viable alternatives for applications. Therefore, we aim to improve technological aspects of the nanostructuring process, not least through the utilization of facilities at the FIRST laboratories at the ETH Zürich. This will be supplemented by the search for alternative materials with possibly superior properties compared to the Nb and NbN films used so far. The fluctuation models also have to be improved and experimentally verified.

[1] A. D. Semenov *et al.*, Physica C, **351**, (2001) 349.

[2] A. Semenov, *et al.*, **Optical Sensing**, volume 5459 (Proc. SPIE Int. Soc. Opt. Eng., 2004), 237.

[3] A. Semenov, *et al.*, Eur. Phys. J. AP, **21**, (2003) 171.

[4] A. Semenov, *et al.*, submitted to Eur. Phys. J., preprint available at cond-mat/0410633.

[5] A. Engel, *et al.*, phys. stat. sol. (c), **2**, (2005) 1668.

Figure 10.3:
Design and realization of a thermal conductivity chip, designed for two separate measurements (dimensions in μm).
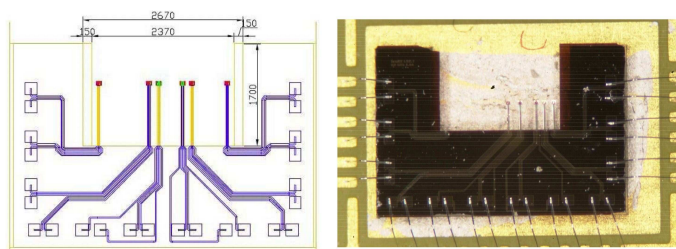
Figure 10.4:
Design and realization of a heat-capacity chip, designed for two separate measurements (dimensions in μm).
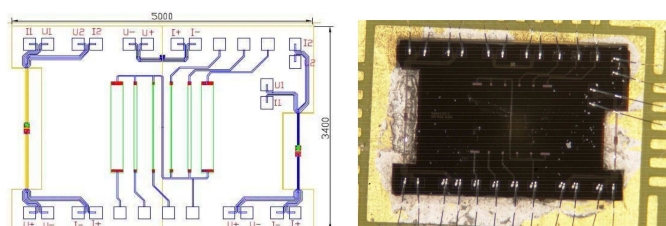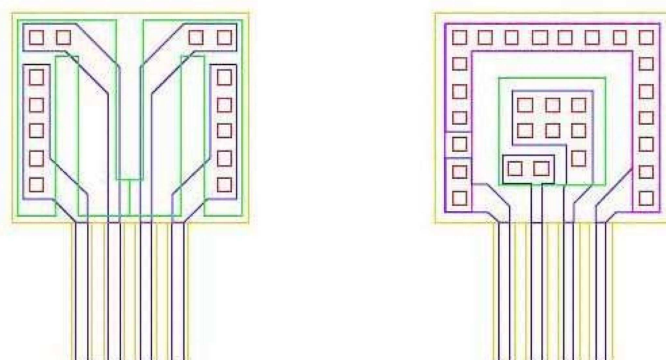
Figure 10.5:
Design and realization of a heater (left) and a thermometer (right). The heater is a p-doped surface, the thermometer is a p-n junction of the same area (78×88 μm^2). (Silicon part in yellow, metallic part in blue, the doped areas are accentuated in purple (n) and green (p), the red squares are the contact pads.)

10.2 Design and development of miniaturized thermal conductivity and heat-capacity experiments

We have designed several miniaturized experiments on silicon chips that will enable us to perform more accurate thermal conductivity and heat-capacity measurements on microscopic samples. A standard steady-state heat flow configuration and an AC calorimetry experiment have been miniaturized to an area of 2.5×3.4 mm^2.

We fabricated these chips on a standard Silicon wafer (in collaboration with CSEM, Neuenburg). For both types of measurements we used p-n junctions as thermometers and p-doped areas as heaters (see Fig. 10.3, Fig. 10.4 and Fig. 10.5). Programming and calibration work will be subject of a future bachelor or a masters thesis.

10.3 Bose-Einstein condensation of magnons in the S=1/2 spin system TlCuCl$_3$?

Last year we have reported on measurements of the thermal conductivity of TlCuCl_3 in its magnetically ordered state, i.e. in magnetic fields above $\mu_0 H_c \approx 5.5$T at low temperatures. These measurements were motivated by the search for the manifestation of a Bose-Einstein condensation of magnons (1) that should lead to an enhanced heat transport as it is ob-

served in superfluid helium.

However, in our experiments we could not detect any clear, significant enhancement in the thermal conductivity of $TlCuCl_3$. This may be due to the fact that a low spin-lattice relaxation rate $\frac{1}{T_1}$ does not allow for an efficient coupling of the spin system to the external heat source that heats up the crystal lattice in such an experiment (2). Therefore we decided to design an alternative experiment with the aim to excite the spin system directly. A general feature of condensates is the existence of collective excitations of the quasi-particles. One such a mode is called *second sound*. This phenomenon can be regarded as an oscillation in the local density of magnons creating a standing entropy or temperature wave, in analogy to standing entropy waves observed in superfluid helium. Given the crystal dimensions and the dispersion relation of the magnons in the condensate state (3), such standing wave oscillation frequencies should be of the order of 100 kHz and larger.

We have built a Wheatstone-like bridge set-up to detect possible absorption resonances upon the formation of such standing waves. The probe is composed of two branches of identical coils and resistors, respectively. By sweeping the frequency of the signal and measuring the voltage difference ΔU between the two branches we can detect changes in the self inductance of the coil containing the sample. Such changes are expected as soon as the crystals absorbs energy from the electromagnetic field when a resonance phenomenon occurs. At present we reach a voltage sensitivity of 40 nV, which corresponds to changes in the self inductance of one part in 10^8.

[1] T. Nikuni *et al.*, Phys. Rev. Lett. **84**, 5868 (2000).

[2] O. Vyaselev *et al.*, Phys. Rev. Lett. **92**, 207202 (2004).

[3] Ch. Rüegg *et al.*, Nature (London) **423**, 62 (2003).

10.4   Vortex phases in type-II superconductors

Last year we had investigated the magnetic phase diagram of V_3Si using a high-accuracy differential thermal analysis (DTA) method (1), and we detected a variety of thermal effects that may be ascribed to the formation of different vortex phases. However, we have not yet been able to prove that these effects are signatures of a true thermodynamic phase transition. Since the vortex configurations in V_3Si are expected to be out of thermodynamic equilibrium, we decided to perform so-called "vortex-shaking" experiments (i.e. the application of a small AC magnetic field perpendicular to the main field direction), which have been shown to be effective to drive non-equilibrium vortex states into a thermodynamic equilibrium (2; 3; 4; 5). Because the AC-field coils were not part of the initial design of our experiment and a respective upgrade turned out be unsatisfactory

due to large induced screening currents, we decided to build an entirely new heat-capacity probe with many significant improvements compared to the older versions. The new measuring cell is suspended with nylon threads, leading to a better thermal decoupling of the cell. A clamp mechanism enables quick cooling, and two small AC-field coils are mounted on adjustable holders forming a split coil system, with the sample platform placed in between the two AC-coils (see Fig. 10.6).

Figure 10.6:

New heat-capacity probe with suspended measuring cell and AC-coils.

Besides continuing the investigations of the phase diagram of V_3Si using this AC-shaking technique, we also intend to test a theory on the "vortex-shaking" effect by Brandt and Mikitik (5). Consider a thin superconducting strip, with a constant homogeneous external magnetic field H_a directed perpendicular to the plane of the specimen (i.e. along z), and an AC-magnetic field $h\cos(\omega t)$ along x, i.e. perpendicular to H_a and to the screening currents inside the sample (see Fig. 10.7). The currents flowing in the critical state of the strip generate a nonuniform distribution of the magnetic induction $B_z(x)$. The AC field periodically tilts the vortices in this state. However, at each point x with a nonzero sheet current $J(x)$ (the current density integrated over the thickness d), the tilt is not symmetric relative to the central plane of the strip, $z = 0$, and during each cycle of the AC field, the asymmetry leads to a shift of the vortices towards the center of the strip ($x = 0$). This process that tends to equilibrate $B_z(x)$ is called flux line "walking" and is illustrated in Fig. 10.7. Quantitatively, vortex shaking in a thin strip should be effective for $h > J_c/2$ (5), irrespective of the shaking frequency ω. As J_c decreases with increasing temperature T, an equilibrium state should be reached as soon as $J_c = 2h$. The effect of the vortex-shaking process has already been observed in magnetization experiments (3; 4), and it should be observable in our experiment as well.

We intend to test the above quantitative predictions on a twinned $YBa_2Cu_3O_7$ single crystal with T_c = 91 K and $m = 8.18$ mg, that does not show the first-order vortex-melting transition as observed in clean, untwinned samples with weaker vortex pinning (work in collaboration with Th. Wolf, Forschungszentrum Karlsruhe). We have estimated the critical-current density j_c of this crystal from magnetization measurements and using the standard Bean model (see Fig. 10.8). At the expected melting transition, T = 82 K in $\mu_0 H_a$ = 5 T, j_c is already vanishingly small and well within reach of the field amplitudes of our AC-split-coil arrangement. Consequently, the equilibrium first-order melting transition of the vortex lattice should become observable also in this twinned $YBa_2Cu_3O_7$ single crystal.
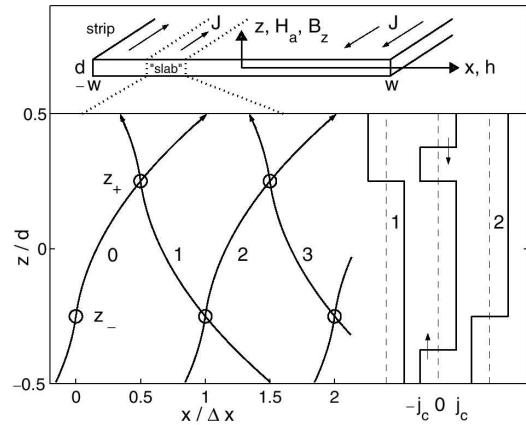

Figure 10.7:
Strip geometry to illustrate the flux line "walking" from left to right through a section of the strip, shown at times $t\omega/\pi = $ 0, 1, 2, 3 [5].
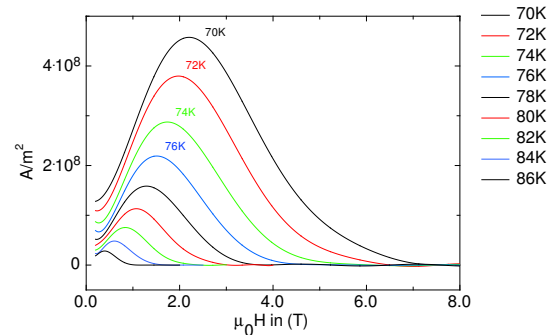

Figure 10.8:
Field dependence of the critical-current density j_c of a twinned $YBa_2Cu_3O_7$ single crystal for different temperatures.

[1] A. Schilling and O. Jeandupeux,
Phys. Rev. B **52**, 9714 (1995).

[2] M. Willemin *et al.*,
Phys. Rev. B **58**, R5940 (1998).

[3] M. Willemin *et al.*,
Phys. Rev. Lett. **81**, 4236 (1998).

[4] N. Avraham *et al.*,
Nature (London) **411**, 451 (2001).

[5] E. H. Brandt and G. P. Mikitik,
Phys. Rev. Lett. **89**, 027002 (2002).